Prepared for submission to JINST

Measurement of the mean excitation energy of liquid argon

M. Strait

Fermilab, PO Box 500, Batavia IL 60510, USA

E-mail: mstrait@fnal.gov

Abstract: The mean excitation energy (I-value) of liquid argon is a critical input for energy estimation in neutrino oscillation experiments. It is measured to be (205 ± 4) eV using the range of 402.2 MeV protons from the Fermilab Linac. This compares to the author's recent evaluation of (197 ± 7) eV based on a combination of an oscillator strength distribution analysis, gaseous argon range measurements, sparse stopping power data on solid argon, and an extrapolation of data on the effect of phase from other substances. Using all sources of information, we recommend a value of (203.0 ± 3.2) eV for liquid argon, which is significantly higher than 188 eV, from ICRU-37's gaseous argon evaluation, commonly used in Monte Carlo codes such as Geant4.

Keywords: Interaction of radiation with matter, Neutrino detectors

ArXiv ePrint: 25XX.XXXXX

arXiv:2501.10550v1 [physics.acc-ph] 17 Jan 2025

Contents

1 Introduction **2**

2 Experimental setup **2**

3 Data collection **4**

4 Fit procedure **5**

5 Systematic uncertainties **6**

5.1 Scintillator 6

5.2 Beam 8

5.3 Monte Carlo code consistency 8

5.4 Materials accounting 9

5.4.1 Aluminum vessel 9

5.4.2 Copper strips 10

5.4.3 Insulation 10

5.4.4 Density of liquid argon 11

5.4.5 Other material adjustments 12

5.5 Multiple Coulomb scattering 12

5.6 Other I-values 13

5.7 Other physics uncertainties 13

5.7.1 Hadronic cross sections 13

5.7.2 Shell corrections 14

5.7.3 Delayed energy 14

5.7.4 Straggling 14

5.8 Alignment 14

5.8.1 Vessel alignment 14

5.8.2 Scintillator position 15

6 Conclusions **15**

7 Acknowledgments **16**

[1]

1 Introduction

Neutrino detectors such as DUNE [1] depend on knowledge of the mean excitation energy, also known as the *I-value*, of liquid argon to estimate neutrino energy. The I-value controls the stopping power of a substance for charged particles in the energy range where the Bethe formula is valid, $0.1 \lesssim \beta\gamma \lesssim 1000$ [2]. In a liquid argon neutrino detector, the primary method to determine muon energy is by range, and the primary method of calibrating the calorimetric response is to use the minimum ionizing portion of muon tracks. Each of these relies on correct simulation that depends on liquid argon's I-value. Typically there are no calibration points in the GeV range that can be used to mitigate an incorrect I-value. While near detectors cancel out neutrino flux and neutrino cross section uncertainties in long-baseline analyses, they do not cancel out energy reconstruction uncertainties.

ICRU Report 90 [3] gave the I-value of gaseous argon as (187 ± 3) eV. The present author has re-evaluated the world data on gaseous argon and recommends the same central value with a larger uncertainty: (187 ± 4) eV [4]. No previous recommendation had been given for liquid argon, with mainstream simulation packages such as GEANT4 assuming the same I-value for all phases, and using the older value of 188 eV from ICRU Report 37 [5]. In Ref. [4], the author recommended (197 ± 7) eV, based on very sparse solid argon data and an extrapolation from other substances whose stopping power has been measured in both the gaseous and condensed phases. The stopping power of liquid argon has not previously been measured.

We report on the first measurement of I-value of liquid argon. Sections 2 and 3 describe the experimental setup and data set. Section 4 explains the fitting procedure, while section 5 presents an analysis of the systematic uncertainties. Section 6 gives our recommendation for the I-value and concludes.

2 Experimental setup

A vessel containing liquid argon was exposed to the Fermilab Linac beam at the Irradiation Test Area (also known as the MuCool Test Area). See schematic and photograph in figure 1. The beam is at a fixed energy, and is pulsed. For this measurement, pulses came once a minute with a length of 7 μs, each pulse consisting of 7×10^{11} protons.

The primary beam from the Fermilab Linac is H^- with a central energy of 402.7 ± 0.2 MeV. This compares to the design H^- energy of 401.5 MeV [6]. The beam energy was determined by using the known circumference and RF frequency of the Booster, which receives protons from the Linac, and cross-checked by further characteristics of the accelerator chain. The Linac beam energy is monitored to ensure it can be injected into the Booster and is stable to 0.1 MeV. The beam kinetic energy has an approximately Gaussian distribution with an RMS of 0.50 ± 0.05 MeV [7]. After stripping in a 0.05 mm titanium beam window, the resulting protons entering the experimental setup have a mean kinetic energy of 402.2 ± 0.2 MeV. The stripped electrons, with kinetic energy of 220 keV, are rapidly stopped at the upstream end of the experimental setup. Simulation shows that their secondaries contribute only on order of 10^{-7} as much energy in the downstream detectors as the protons. They are neglected from here on.

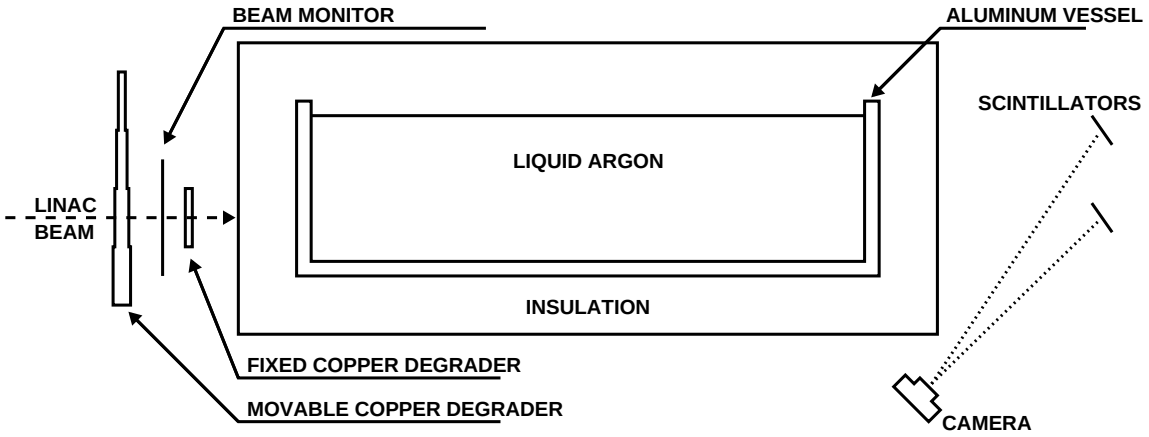

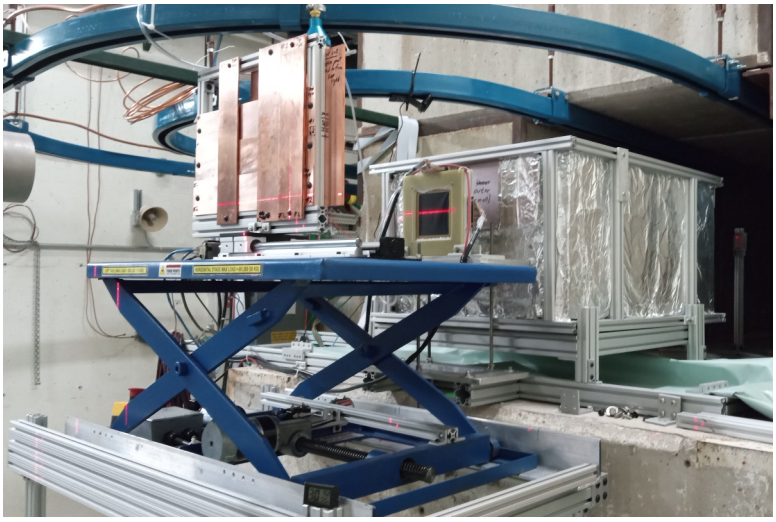

Figure 1. Top: Experimental schematic of experiment carried out at the Fermilab Irradiation Test Area. Not to scale. Bottom: photograph of same.

The beam profile was monitored by a wire chamber upstream of the vessel. It is close to Gaussian with an RMS of 1.2 cm both horizontally and vertically. The beam pipe is 10 cm in diameter.

The thickness of the liquid argon and its vessel in the beam direction was chosen to be somewhat less than enough to stop the protons. The argon vessel was a rectangular open-topped aluminum 6061 tub with interior length, in the beam direction, at 87 K, of 654.1 mm (656.6 mm at room temperature). The liquid argon was obtained from Airgas and was industrial grade, 99.997% pure. The interior width was 220 mm and the height 160 mm. The walls of the vessel were 17.76 mm thick. The vessel was surrounded by Foamular-250 polystyrene insulation boards, with 51 mm at the front and back in the beam direction, 178 mm on the right and left sides, 203 mm below and 229 mm above. The insulation was sufficient to keep an adequate volume of liquid argon for many hours at a time without active cooling. The insulation was wrapped in aluminum foil for fire protection, but not the section directly in the path of the beam.

Immediately upstream of the argon vessel were two fixed copper strips with total thickness

6.33 mm. Their purpose is to reduce the beam energy to better match the size of the liquid argon vessel. A copper assembly 0.5 m further upstream contained 20 thicknesses of copper, evenly spaced from zero to 15.17 mm, each of which could be remotely moved into the beam to scan over beam energies. In this way, the mean proton energy entering the vessel's front face could be adjusted from 361 MeV (the greatest copper thickness) to 390 MeV (the least copper thickness). The Bragg peak and subsequent rapid decrease in transmittance is observed as a function of increasing copper thickness.

The transmittance of the materials in the beam was measured by two ceramic scintillators 0.5 m downstream of the vessel, one directly on the beam axis and the other 14 cm off-axis. Made by Advatech, the scintillators are 50 mm by 50 mm by 1 mm. They are 99.5% aluminum(III) oxide doped with chromium(III) oxide, known as *chromox*, with density 3.85 g/cm^3 [8]. Both scintillators were observed by a single commodity video camera, a Logitech C920, positioned 1.2 m off the beam axis. The scintillators were angled 30° towards the camera with respect to the beam axis. Immediately downstream of the vessel is a stack of concrete shielding blocks with a "cave" 1 m wide by 1 m tall along the beam path that leads to the beam dump. The scintillators were positioned inside this cave, which, compared to an open configuration, slightly increases the flux of secondary particles they observe along with the primary protons.

3 Data collection

Data was obtained for 9 thicknesses of copper across a total of 31 pulses, with between 1 and 6 pulses per thickness. Unforeseen circumstances prevented further data taking. A more even distribution of data across all 20 thicknesses of copper would have been desirable, but this data is sufficient to make a measurement.

Camera images were analyzed to determine the relative amount of ionization in the scintillator from each pulse. As shown in figure 2, images contained both scintillation light and background from secondary beam particles directly striking the camera. The former registers almost exclusively in the camera's red pixels, while the latter appears equally in all three color channels, since radiation directly ionizes the CMOS sensors, bypassing the color filters. By subtracting the signal in blue and green pixels from that in the red pixels, the scintillation light is isolated. Empirically, subtracting the green channel scaled by 0.44 and the blue channel scaled by 0.59 yielded the best results, as judged by regions of the images away from the scintillator. The resulting pixel values (including those that are negative after subtraction) are then summed for each scintillator panel.

The camera gain was set to avoid saturation in any of the pixels for the on-axis scintillator. However, this meant that the signal observed in the off-axis scintillator was very weak. The off-axis data is nevertheless sufficient to cross-check the main result from the on-axis scintillator.

As the scintillator emission time is comparable to the camera frame rate, 30 frames per second, the signal from the frame containing the pulse and the following frame were summed. The following frame is free of beam background, but only contains a small minority of the light, so cannot be used alone to avoid the background.

Differences in the measured signal from pulse to pulse can be caused by variations in the beam intensity, the number of particles striking the camera in the pixels observing the scintillator, and effects related to the camera readout. Collectively these will be referred to as statistical uncertainty.

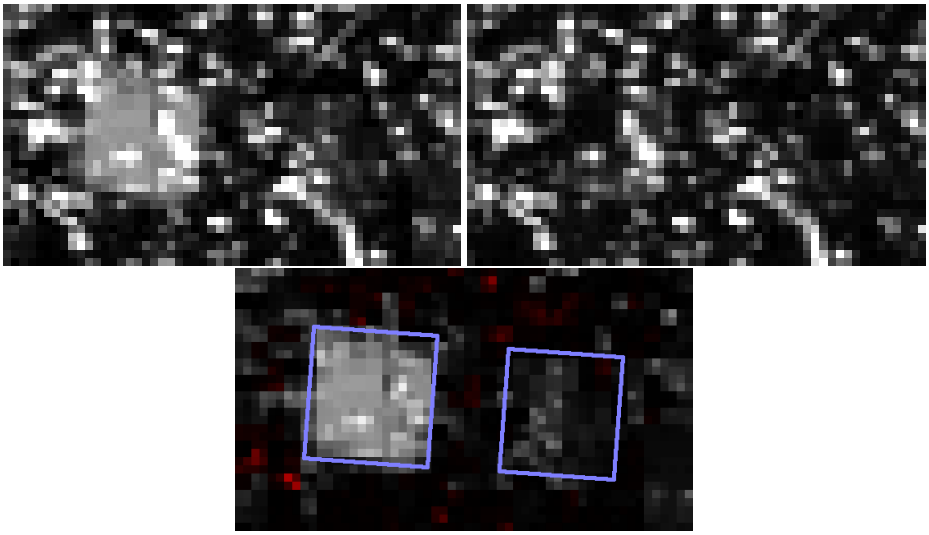

Figure 2. Top left: Example of raw data, red channel. Top right: same, 44% of green channel added to 59% of blue channel. Bottom: subtraction of above two images, with outlines showing the positions of the two scintillator squares. Pixels with negative values after subtraction are shown in red. All three images are displayed with increased contrast for clarity.

The statistical uncertainty has been estimated via the spread of measurements using the same copper absorber thicknesses. It is strongly subdominant to the systematic errors that will be discussed in the following sections.

4 Fit procedure

The experimental setup was simulated using GEANT4 v11.2.1 [9]. See figure 3. The physics list `FTFP_BERT_EMZ` was used, where `EMZ` is also known as EM `Opt4`, and provides the best EM physics available in GEANT4.[2] For all materials, the `DensityEffectCalculatorFlag` was set to obtain the best available treatment of the Fermi density effect. At the relevant energies, this has no effect for argon but a small effect for the aluminum vessel and copper strips, since they have more loosely bound electrons.

The experiment was simulated with the I-value of liquid argon set to 181 eV, 189 eV, 197 eV, 205 eV, and 213 eV and with each of the 20 copper absorber thicknesses, with 10^7 to 10^8 protons simulated in each case, with higher statistics used for points providing more information to the fit, such that the uncertainty from Monte Carlo statistics is negligible. The normalization of the signal is a free parameter in the fit; i.e. we do not attempt any a priori calibration of the scintillator yield or camera's efficiency. As a very good approximation, the transmission as a function of copper absorber thickness differs from one I-value to another only by a horizontal translation and a normalization (see figure 4). Therefore, the shape of this curve is used as a template in the fit which extracts the experimental I-value from the data. In the fit, there are three free parameters — the overall normalization, the left-right shift (absorber thickness), and the up-down shift (background normalization). For the off-axis fit, the background normalization is fixed to the Monte Carlo

[2] https://geant4-userdoc.web.cern.ch/UsersGuides/PhysicsListGuide/html/electromagnetic/

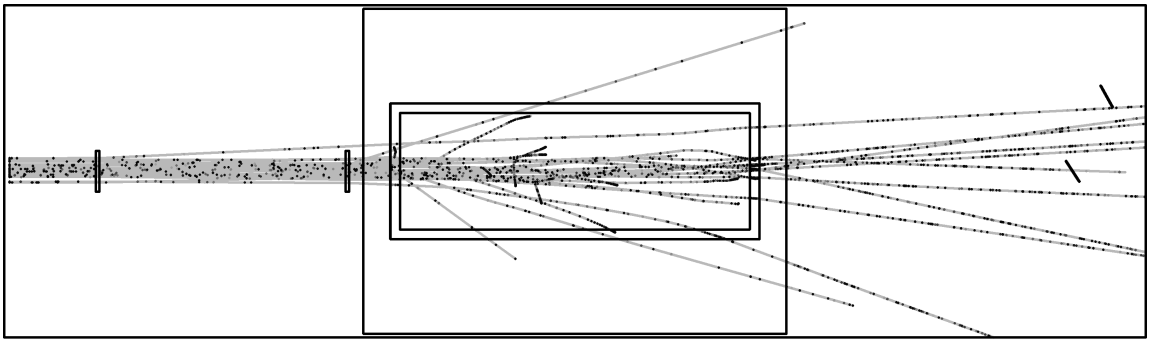

Figure 3. Top view of a GEANT4 simulation of 25 protons in the configuration using 11.70 mm of copper degrader, including the fixed 6.33 mm degrader immediately upstream of the vessel. Gray lines are the proton trajectories and the black points on the lines are GEANT4 steps. Secondary particles and the concrete shielding blocks are not shown. The on-axis and off-axis scintillators are visible on the right side.

prediction, while on the on-axis fit, the data is allowed to constrain it. The results are shown in figure 5.

For the on-axis result, it was found that the data prefers a sharper Bragg peak than the prediction. The largest discrepancy arises from the data taken at 8.8 mm, although the data at other positions also tends to prefer a sharper peak. We investigated whether the 8.8 mm data could be flawed, but did not find any evidence of this. For instance, it was not taken first or last, and the data from pulses immediately before and after it (11.9 mm and 15.1 mm, respectively) lies directly on the best fit line. Beam monitoring did not show the 8.8 mm pulses to be abnormal, and we could independently confirm this from the magnitude of the beam background observed in the obtained images. This discrepancy will be discussed further in sections 5.1, 5.2 and 5.3.

Given this unexpected feature, in determining the central value of our result, we exclude the data from 8.8 mm to lessen the discrepancy between data and simulation. Figure 5 shows the difference in the fit with and without this exclusion. Note that the curves almost exactly coincide for the falling edge around 16 mm. It is primarily this edge which sets the I-value, making the details elsewhere relatively unimportant to the result. The extracted I-value differs by only 0.5 eV between these two fits, and another 0.5 eV if the next group of data points at 11.1 mm is also excluded. This problem either does not occur in the off-axis data, or is obscured by the large uncertainties.

The independent results of $(205 \pm 2(\text{stat}))$ eV and $(212 \pm 7(\text{stat}))$ eV from the on-axis and off-axis scintillators, respectively, are in good agreement.

5 Systematic uncertainties

Many sources of systematic error were investigated. All of the uncertainties discussed in this section are summarized in Table 1.

5.1 Scintillator

According to the manufacturer and CERN-PS-90-42-AR [10], chromox scintillator has an extinction coefficient of (8 ± 1) cm^{-1} for its peak light production frequency of 693 nm. However, a more recent study by Cook, Tresca and Lefferts 2014 [11] measured the attenuation length using transmission of

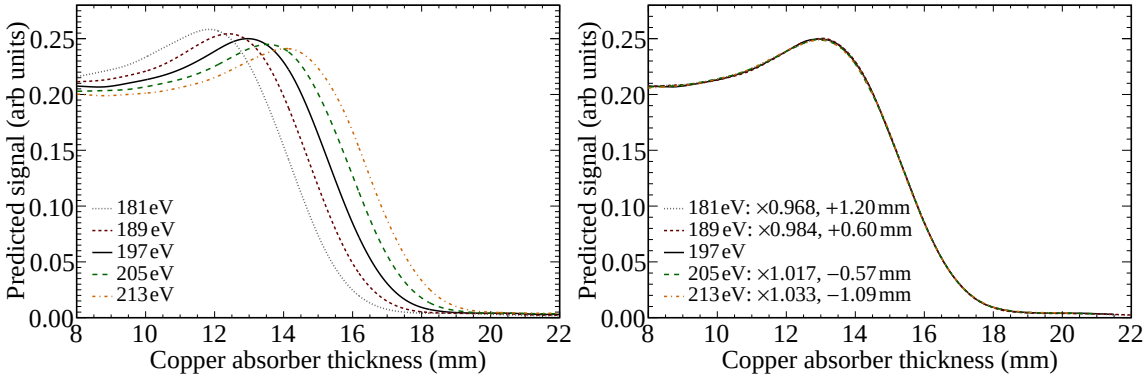

Figure 4. Predicted signal (with no scintillator quenching effect applied) as a function of I-value, showing that only the normalization and horizontal position of the curve change with I-value, as a good approximation. Left: the raw predictions for five I-values. Right: the same predictions, scaled and translated to match the curve for 197 eV.

633 nm light to be (0.05 ± 0.01) cm, i.e. an extinction coefficient of (20 ± 4) cm^{-1}, and also found that including a Birks' quenching factor gives a better fit to proton irradiation data. Their reported best fit was for a Birks' constant of 2.33×10^{-2} g MeV^{-1}cm^{-2} and attenuation length of 0.058 cm or 0.057 cm (both values are quoted). This quenching constant is large compared to typical values for inorganic scintillators, although not outside what has been measured before [12].

However, the effect of scintillator quenching is to flatten the Bragg peak, since quenching suppresses light production from low energy protons. This is substantially at odds with our data, which prefers a sharper Bragg peak than Monte Carlo predicts even without quenching. A resimulation of Cook's setup was performed to investigate this discrepancy. Using the data from their Figure 2, we find that a much smaller Birks' constant along with a shorter attenuation length fits the data somewhat better (see figure 6). Since they viewed their scintillator from the back, both parameters result in loss of light for protons with a range shorter than the scintillator thickness, and so the two effects cannot be readily separated.

For analyzing our data, we adopt a Birks' constant of 0.25×10^{-2} gMeV^{-1}cm^{-2}, halfway between what our data prefers, zero, and the value we fit in figure 6. Varying this between zero and 0.5×10^{-2} gMeV^{-1}cm^{-2} gives our estimate of the systematic uncertainty stemming from quenching, ±0.8 eV.

Several rather different proposals for the value of the attenuation length are now in play. At one extreme is the manufacturer's value of 0.125 cm, there is Cook's value of 0.05 cm, and our value of 0.03 cm which, combined with a small value of Birks' constant, gives a closer fit to both their data and ours. Changes in the scintillator attenuation length are almost exactly degenerate with an overall left-right shift of the predicted light curve, as it is equivalent to adding or subtracting material in the protons' path. The difference in inferred I-value between the extremes of the possible attenuation values is 1.0 eV. We take 0.05 cm as the nominal attenuation length, assume a uniform PDF over the range and claim an uncertainty of 0.4 eV.

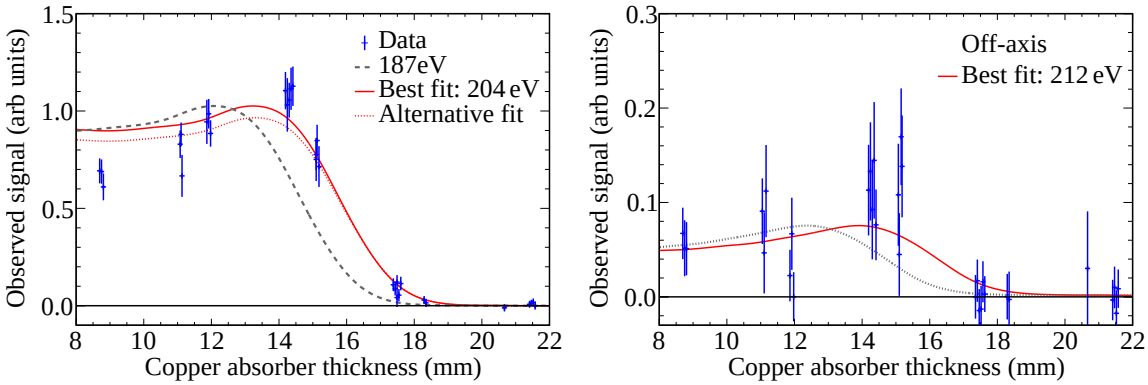

Figure 5. Left: Experimental data for on-axis scintillator (crosses) with a comparison to GEANT4 simulations using $I = 187$ eV (the ICRU-90 value for gaseous argon) and 204 eV (the best fit value). The solid red curve shows the primary fit, which excludes the data at 8.8 mm, while the dotted curve is a fit including these points. Each cluster of data points is for a single copper absorber thickness and have been given slight horizontal separations to display the uncertainties. Right: the same for the off-axis scintillator with its fit result of 212 eV, showing only the primary fit.

5.2 Beam

The uncertainty in the central energy of the beam of 0.2 MeV leads to an uncertainty on the I-value of 1.5 eV, making it one of the dominant uncertainties. In contrast, the measured I-value is quite insensitive to the details of the energy spread, with a shift of less than 0.1 eV resulting from the (0.5 ± 0.05) MeV uncertainty on the beam energy width. Since our data favors a sharper Bragg peak than the Monte Carlo predicts, one could wonder if the beam energy profile is narrower than what was modeled. However, nearly all of the spread of the peak is caused by energy straggling in the experimental materials and not the initial energy profile of the beam. Even if the beam were monoenergetic, only a small fraction of the discrepancy would be explained by it.

The details of the energy profile are likewise not important; for instance if the profile, instead of a single Gaussian with an RMS of 0.5 MeV, were a sum of two equally weighted Gaussians, one with RMS 0.5 MeV and one with RMS 2.0 MeV, the result for the I-value shifts by only 0.12 eV.

The nominal beam spot size is 1.2 cm RMS, verified by beam monitors during the run. Even large changes to this size have a negligible effect on the inferred I-value.

5.3 Monte Carlo code consistency

We reran the simulations using MARS version 2024-04-25 [13], CERN FLUKA version 4-4.0 [14], and PHITS version 3.34 [15]. See figure 7. MARS was run in MCNP mode for neutron transport below 14.5 MeV, and otherwise in its default configuration. The hadronic cross section was reduced by 5% to better match GEANT4. A "Z-sandwich" geometry was used, modeling the experimental design with a series of simple slabs; this is a good approximation given the large transverse extents of the experimental components, and allows for much better code performance. The dose on the scintillator scored in a number of radial layers and a weighted sum was used to determine the dose for the true geometry. FLUKA was run in PRECISION mode. PHITS was run with Landau-Vavilov energy straggling (`nedisp = 1`), the NMTC model [16] for multiple Coulomb scattering (`nspred`

Table 1. Systematic uncertainties. Materials accounting includes uncertainties on the densities and thicknesses of all materials.

Uncertainty	eV
Scintillator & camera	±1.6
Beam energy	±1.6
Monte Carlo code consistency	±1.4
Materials accounting	±1.2
Multiple Coulomb scattering	±1.0
Aluminum & copper I-values	±0.7
Other physics	±0.5
Alignment	±0.4
Total systematic uncertainty	±3.3
Statistical uncertainty	±1.6
Total uncertainty	±4

= 1), the ATIMA model for energy loss (`ndedx = 1`), and using `e-mode = 1` for low-energy neutrons.

The other Monte Carlo codes predict slightly shorter or longer proton ranges than GEANT4 given the same I-value, meaning that analyzing the data using them results in, respectively, higher or lower I-values. FLUKA and MARS each give a result 1.6 eV higher than GEANT4, while the answer from PHITS was 1.0 eV lower. As is visible from the plot, the largest difference between the codes is on the left side, before the peak, although it is the falling edge on the right side which gives the range. The PHITS result is in somewhat better agreement with the low data points at 8.8 mm, but the difference is not enough to bring data and simulation together.

Differences between Monte Carlo codes can result from such a wide variety of causes that it is not easy to pin down the source. In each case, we used the most accurate options available so far as our expertise allowed. It can be seen that the difference between various codes is similar to the difference obtained by using different options within GEANT4, e.g. the multiple scattering model. It is reasonable to suppose that similar choices between several available approximations is the reason for the differences from one code to another. We conservatively choose to take the RMS of the results from the four codes, 0.9 eV, as an additional systematic uncertainty, although this may represent double counting to some extent. The central value obtained from GEANT4 is retained as our central value, however if the reader would prefer to use the mean of the four codes, add 0.7 eV to our stated experimental result.

5.4 Materials accounting

5.4.1 Aluminum vessel

The front and back walls of the aluminum tub are (17.83 ± 0.03) mm thick at room temperature. At the boiling point of argon, 6061 aluminum linearly contracts by a factor of 0.99621 ± 0.00015 [17] to (17.76 ± 0.03) mm. Given the thermal conductivities of the insulation and aluminum, the aluminum's temperature is uniformly within 0.1 K of the argon temperature. The uncertainty associated with

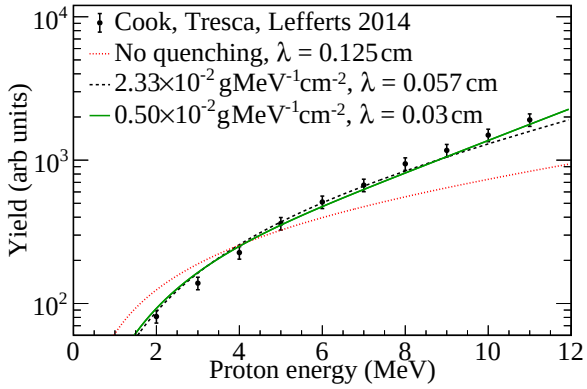

Figure 6. Data from Ref. [11] shown along with our re-simulation of their setup for three scenarios: no quenching and the manufacturer's quoted attenuation length, Cook's best fit, and our model with much less quenching and which fits the data better by 0.9 units of χ^2.

the amount of contraction is negligible compared to the uncertainty of the thickness at room temperature. The uncertainty in the total thickness of aluminum of 0.06 mm has 35% the stopping power of the same thickness of copper. From the Monte Carlo simulation described above, each additional millimeter of copper degrader needed to stop the beam corresponds to an additional 15 eV in liquid argon's I-value. The uncertainty in aluminum thickness therefore gives an uncertainty in the I-value of 0.3 eV.

Given the specification of 6061 aluminum, there is some freedom in its elemental composition. The first-order effect for the stopping power is the material's mean Z/A. The allowed range is 0.12%, giving an uncertainty in liquid argon's I-value of 0.06 eV. The density of our particular aluminum was not measured. We take 6061 aluminum density to be (2.69 ± 0.01) g/cm^3 [18], and further taken as uncorrelated to the uncertainty in its elemental composition, leading to an uncertainty of 0.6 eV. The interior length of the aluminum vessel has a tolerance of 0.25 mm. The resulting uncertainty in the thickness of liquid argon leads to an I-value uncertainty of 0.3 eV. The aluminum's density dominates the uncertainty from the aluminum vessel, which is 0.8 eV in total.

5.4.2 Copper strips

The density of the copper strips is taken to be (8.94 ± 0.02) g/cm^3, using a combination of public data on density of copper and our own measurements of copper blocks from the same supplier. The copper's temperature was the temperature of the air in the hall, 13°C. The difference in its density at this temperature and at the nominal 20°C is negligible. Each strip's thickness is known to ±0.008 mm, and we conservatively assume full correlation of this uncertainty from strip to strip. The resulting uncertainties on the I-value of liquid argon from density and thickness are 0.5 eV and 0.3 eV, respectively.

5.4.3 Insulation

The insulation is Foamular-250 polystyrene, with a manufacturer-quoted minimum density of 0.0248 g/cm^3. Taking the insulation to have (0.027 ± 0.002) g/cm^3 leads to an I-value uncertainty of 0.4 eV.

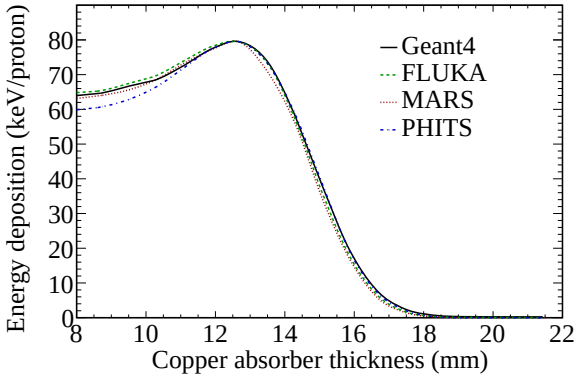

Figure 7. Comparison of several Monte Carlo codes. The prediction of energy deposition in the on-axis scintillator is shown. The MARS, FLUKA and PHITS results have been scaled by −2.2%, +9.6% and −0.6%, respectively, so that the peak matches GEANT4.

The inner surface of the insulation is at the temperature of the aluminum vessel, approximately the boiling point of liquid argon, while the outer surface is at the ambient 13°C. The thermal contraction of the insulation was not analyzed in detail, since its change in density between the ambient temperature and liquid argon temperature, 4%, is less than the uncertainty of its room temperature density.

5.4.4 Density of liquid argon

Because the argon was not actively cooled, it was at its boiling point, which is significantly affected by the atmospheric pressure. During the experimental run, the sea-level pressure recorded by the weather station at the O'Hare airport 33 km to the east-northeast was 1004 hPa and by the Dekalb/Cortland airport 38 km to the west-northwest was 1005 hPa. Other area weather stations agreed within 1 hPa. Taking the mean of these, and converting from the reported sea-level pressures to the pressure at the experiment's elevation, 225 m, gives 978 hPa. The uncertainty on the readings from each weather station is conservatively taken to be 0.7 hPa, corresponding to the required ±0.02 inHg accuracy required by the United States Federal Meteorological Handbook No. 1, 2019 [19]. The accuracy of converting the sea level pressure to the local pressure at Fermilab's altitude is better than 1 hPa [20]. The vessel was unpressurized, with insulation placed loosely on the top, such that the pressure difference between the interior and exterior was much less than 1 hPa. Overall, we take the pressure to be (978 ± 1) hPa.

From Ref. [21], given the pressure, the argon's boiling point was (86.97 ± 0.02) K, where the uncertainty of the pressure dominates over the uncertainty of the correspondence between the pressure and the boiling point, given a 0.04% uncertainty in the vapor pressure as a function of temperature. This is significantly lower than argon's standard boiling point of 87.303 K.

Correspondingly, again using Ref. [21], its density is (1.3975 ± 0.0004) g/cm^3, above the density at standard pressure of 1.3953 g/cm^3. The uncertainty has equal contributions from the uncertainty in the boiling point and the uncertainty of ±0.02% from the correspondence between temperature and density. The density uncertainty results in an I-value uncertainty of 0.4 eV.

5.4.5 Other material adjustments

The vessel was filled with liquid argon with a total depth of 16 cm. Data was taken between two and four hours after the fill. Previous tests without beam showed that the loss rate of liquid argon is 0.3 cm per hour. Each beam pulse adds additional heat, but this effect increases the evaporation rate by only 0.1%. Therefore, we estimate that the argon level varied from 15.4 cm to 14.8 cm during the experimental run. Monte Carlo simulations used for the fit assumed a depth of 12 cm, but we find no significant differences in simulation results for depths between 11 cm and 16 cm. Even at 11 cm, there is continuous argon for all straight-line paths from the beam pipe to the scintillator, but small modification in transmission begin to occur because protons which are scattered upwards into the air have no significant chance of being scattered back down towards the scintillator.

Although the liquid argon is at its boiling point, the insulation was chosen to ensure that evaporation would occur only at the surface of the liquid, and not through nucleate boiling, meaning that the path the protons traverse contains only argon in the liquid phase. Tests of the vessel with liquid nitrogen showed only very limited nucleate boiling, even with the lid removed and the top of the nitrogen exposed to room temperature air. Liquid argon has a higher density, higher boiling point and larger heat of vaporization, all of which reduce its boiling rate relative to nitrogen. Given these observations, we estimate that the protons' mean path length through gaseous argon is no greater than 0.01 mm. This being much smaller than the 0.25 mm tolerance on the vessel's interior length, it has no effect on the measurement.

We also consider the possibility that a thin layer of frost formed between the insulation and the aluminum vessel. During tests when the vessel was constructed, there was no indication of this problem occurring, but it was not possible to inspect the vessel after the beam run. Given the degree of flushness between the aluminum vessel and the insulation, we consider 0.25 mm to be the largest credible thickness of frost. We model the mean case in the simulation, i.e. 0.125 mm of ice on the front and back of the vessel. An uncertainty of 0.2 eV is incurred from the range of possible frost thicknesses.

5.5 Multiple Coulomb scattering

Multiple Coulomb scattering affects the projected range of protons through the liquid argon. Our analysis uses GEANT4's electromagnetic `EMZ` option, also known as `Opt4`. This option uses the best available multiple scattering model in GEANT4: "multiple Coulomb scattering is performed by the `WentzelVI` model and Coulomb scattering by the `eCoulombScattering` model." The `WentzelVI` model implements the algorithm from Fernández-Varea 1993 [22], using the potential form introduced by Wentzel 1926 [23]. This remains an approximation, for instance there are no detailed models of atoms' potentials, only the simple Wentzel form

$$V = \frac{eE}{r} e^{-r/R},$$

where the atomic radius is taken as a continuous function of Z:

$$R = 0.885 Z^{-1/3} a_0 \left[1.13 + 3.76(\alpha Z/\beta)^2\right]^{-1/2}.$$

We compared `EMZ` to GEANT4's single scattering model, in which every Coulomb scatter is simulated independently instead of using an approximate distribution to simultaneously simulate

the effect of many scatters. This is enabled using the `FTFP_BERT_EMZ` physics list, followed by `ReplacePhysics(new G4EmStandardPhysicsSS)`. The single scattering model is extremely CPU intensive to run, being three orders of magnitude slower than multiple scattering. Only one degrader thickness was tested, 15.9 mm, which is the most sensitive to differences in proton range. The results were compatible with EMZ, with single scattering giving a signal $(1.6 \pm 1.2)\%$ larger than EMZ. This is equivalent to a decrease of the I-value by (0.3 ± 0.2) eV, assuming the shape of the complete transmission curve is the same for the two models.

While the single scattering model is naively the most accurate, and has been shown to be so for thin targets, it is difficult to show experimentally for thick targets [24–26]. Given that, and the prohibitively high CPU time needed for a full simulation using it, we retain EMZ as our model for this analysis, as it is the most accurate model that is practical to use. Were the single scattering model the ground truth, it would be reasonable to assign a 0.5 eV systematic error associated with using EMZ instead. However, acknowledging that even the single scattering model still makes use of several approximations, we choose to double this to 1.0 eV.

We also checked the effect of using the default, less accurate, `Opt0` electromagnetic option from the `FTFP_BERT` physics list, which uses the so-called `Urban` model for multiple Coulomb scattering. The `Urban` model uses the Highland approximation for multiple scattering,

$$\theta_{\text{rms, plane}} = \frac{13.6\,\text{MeV}}{p\beta} z\sqrt{x/X_0}[1 + 0.038\log(x/X_0)],$$

which is rapid to compute at the expense of accuracy. It predicts a longer projected range which gives an I-value 5.5 eV lower than inferred from the `EMZ` option. We do not use this rather different result except to note that experiments which rely on absolute particle ranges should certainly use `EMZ` and not the default `Opt0`.

We studied whether a larger or smaller scintillator panel would have resulted in less sensitivity to the details of multiple scattering models. The differences are largest along the beam axis, but not dramatically. Using a scintillator of arbitrarily large transverse extent reduces the differences between Opt0 and Opt4/`EMZ` by only 5%. For a scintillator panel of width 1 cm the difference is 30% larger than for the 5 cm panel. This study suggests that the primary difference in the models is in the projected range rather than the angular distribution.

5.6 Other I-values

Using values from ICRU-37, and interpreting them as being at 90% C.L. as suggested by footnote 10, the I-value of the 6061 aluminum alloy is (167.0 ± 1.2) eV. The resulting uncertainty in the stopping power of the vessel leads to an uncertainty in liquid argon's I-value of 0.2 eV. Similarly, the uncertainty of copper's I-value, ±6 eV, leads to a 0.7 eV uncertainty in this measurement.

5.7 Other physics uncertainties

5.7.1 Hadronic cross sections

While there is some uncertainty on the inelastic scattering cross sections of protons on argon nuclei, these interactions have almost no impact on the measurement, since any proton that participates in such an interaction both tends to lose a great deal of energy, meaning that it no longer can arrive at

the far end of the vessel, and also tends to get scattered at a large angle so that it would not reach the detector regardless. The effect of increasing the hadronic interaction cross section is therefore almost entirely to decrease the normalization of the signal, as a function of beam energy, without changing its shape significantly. An adjustment of 20% from GEANT4's default cross section makes only a 0.1 eV impact on the inferred argon I-value.

5.7.2 Shell corrections

Shell corrections to the Bethe stopping power formula become important at low proton energy. These are difficult to calculate precisely, but are a minor effect for 400 MeV protons. For argon, a low-Z nucleus, the uncertainty on the magnitude of the correction is under 10% [5]. A change in the correction at this level has only a 0.3 eV impact on the I-value.

5.7.3 Delayed energy

For each pulse, we integrate the scintillation light collected for two camera frames, 66.7 ms, which means that there is some sensitivity to delayed processes, including neutron capture and decay of activated materials. However, simulation shows that even when the protons are ranged out, e.g. with 20 mm of copper absorber, 99.8% (99.5%) of the energy deposited in the on-axis (off-axis) scintillator is prompt, i.e. within 1 μs of the beam pulse, making the details of neutron propagation and material activation completely unimportant.

5.7.4 Straggling

To test if GEANT4's model for range straggling — the variation in range for particles with same initial energy — biases the result, the experiment was first simulated with the extreme case of no straggling, such that the only significant variations in protons' energy reaching the scintillator were from differing path lengths due to multiple scattering and from the energy spread in the initial beam. Using these simulations to analyze the data instead of the standard simulations resulted in an downwards shift of 4.7 eV in the inferred I-value. As a less extreme case, the GEANT4 `UniversalFluctuations` model was substituted for more accurate `UrbanFluctuations` model (which is the default for both `Opt0` and `Opt4`/`EMZ`), which resulted in a downwards shift of 0.5 eV. From this, we conclude that further improvements in the straggling model are unlikely to result in shifts of more than half this amount and adopt 0.3 eV as the systematic error from the straggling model, which is negligible compared to the uncertainty from multiple scattering.

Two further options that, in principle, increase GEANT4's accuracy were tested. First, the number of bins per energy decade for the dE/dx table was increased from its default of 20 to 100. No significant change was seen in the output, and the effect on the I-value is less than 0.2 eV. Similarly, the production cuts were reduced from their default value of 0.7 mm to 0.007 mm. Again no significant change was seen and the impact is less than 0.2 eV.

5.8 Alignment

5.8.1 Vessel alignment

All experimental components were aligned to better than 1° with the beam. Any unmodeled misalignment would increase the protons' path length and make the inferred I-value lower. If the

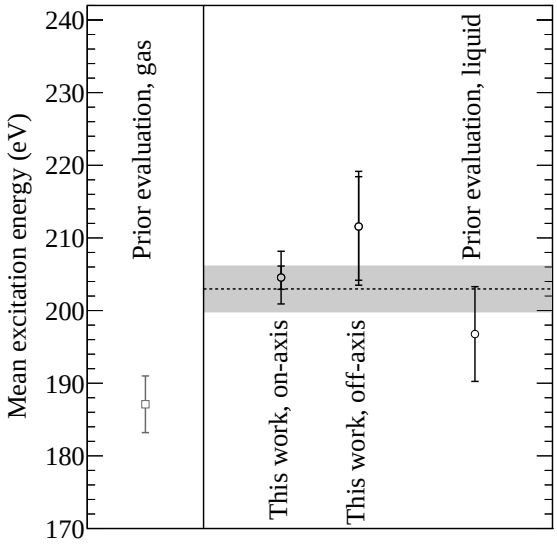

Figure 8. Combination of prior information with these results. The gray band shows the result combining all past and present information. The present result for the on-axis and off-axis scintillators are shown on the right, with statistical and total errors.

liquid argon vessel were misaligned by 1°, it would lower the I-value by 0.3 eV, while a similar misalignment in the copper strips would shift the inferred I-value by less than 0.1 eV.

The vessel's vertical position was determined to 0.5 cm. Similarly to the case of the liquid argon depth, above, there is some slight sensitivity to the vertical position even if all straight-line proton paths lead entirely through argon because protons can scatter from the argon into the aluminum vessel and then back into the argon. Simulation showed that the effect on the I-value is only ±0.2 eV.

5.8.2 Scintillator position

The scintillator panels were placed with an accuracy of 1 cm. By analyzing the data under the assumption that the scintillator is out of its nominal position, it was determined that very little uncertainty is incurred, with the answer only shifting by 0.2 eV.

6 Conclusions

The present results are shown in figure 8 in comparison to the previous evaluations in Ref. [4] for gaseous and liquid argon. The overall result from this measurement combines the on-axis and off-axis scintillator results, assuming full correlation of systematic uncertainties, to arrive at (205 ± 4) eV.

To make our overall recommendation for the I-value of liquid argon, we combine our previous evaluation for liquid argon [4] with the present results. No significant sources of correlated uncertainties were identified between the present measurement and the previous evaluation from Ref. [4], which relied primarily on oscillator strength distributions (i.e. photoabsorption cross sections) and an estimate of the phase effect using previous measurements several other substances in gaseous and condensed forms. Secondary contributions to the previous evaluations come from consideration of

periodic trends, a Hartree-Fock wave function calculation, and a stopping power measurement using natural alpha particles in gaseous argon. Even smaller contributions are from four other stopping power measurements. Some correlation could exist in the treatment of multiple Coulomb scattering in the stopping power measurements. However, this group of measurements collectively make so little contribution that the result is unchanged to the last reported decimal place if they are discounted entirely. Therefore we treat the evaluation and this measurement as independent. To avoid loss of accuracy, we carried all digits through the calculation, using (196.8 ± 6.5) eV for the previous evaluation and (204.9 ± 3.6) eV for the present meeasurement. The combined recommendation is (203.0 ± 3.2) eV.

Using our recommended value rather than the old values of 188 eV or 187 eV shifts energy reconstruction in liquid argon TPCs used for GeV-scale neutrinos by around 0.6%, with the exact shift depending on the analysis method. The inferred value of Δm^2_{32} is directly proportional to reconstructed energy. As DUNE projects a sensitivity to this parameter of around 0.5% (depending on exposure) [27], is it important that a reliable value and uncertainty for the mean excitation energy of liquid argon be used.

7 Acknowledgments

This manuscript has been authored by Fermi Forward Discovery Group, LLC under Contract No. 8924 3024 CSC 000 002 with the U.S. Department of Energy, Office of Science, Office of High Energy Physics. Thanks to Chandrashekhara Bhat, Dali Georgobiani, Carol Johnstone, Matthew King, Alajos Makovec, Lionel Prost, Nathaniel Rowe, Alexander Shemyakin, and Katsuya Yonehara for providing invaluable information and assistance.

References

[1] DUNE collaboration, *Deep Underground Neutrino Experiment (DUNE), far detector technical design report, volume I: Introduction to DUNE*, *JINST* **15** (2020) T08008 [2002.02967].

[2] Particle Data Group collaboration, *Review of particle physics*, *Phys. Rev. D* **110** (2024) 030001.

[3] International Commission on Radiation Units and Measurements, *Report 90: Key data for Ionizing-radiation dosimetry: measurement standards and applications* (2016).

[4] M. Strait, *Evaluation of the mean excitation energies of gaseous and liquid argon*, *JINST* **19** (2024) P01009 [2212.06286].

[5] International Commission on Radiation Units and Measurements, *Report 37: Stopping powers for electrons and positrons* (1984).

[6] C.W. Schmidt, *The Fermilab 400-MeV Linac upgrade*, *Conf. Proc. C* **930517** (1993) 1655.

[7] C.M. Bhat and D.E. Johnson, *Energy spread measurements for 400 MeV Linac beam at Fermilab Booster using a laser notcher system*, in *3rd North American Particle Accelerator Conference (NAPAC2019)*, pp. 868–870, 2019, DOI.

[8] Muon Acceleration R&D collaboration, *Measurement of Transmission Efficiency for 400 MeV Proton Beam Through Collimator at Fermilab MuCool Test Area Using Chromox-6 Scintillation Screen*, *Rev. Sci. Instrum.* **84** (2013) 063301.

[9] J. Allison et al., *Recent developments in Geant4*, *Nucl. Inst. Meth.* **A835** (2016) 186.

[10] C.D. Johnson, *The development and use of alumina ceramic fluorescent screens*, Tech. Rep. CERN-PS-90-42-AR (1990).

[11] N. Cook, O. Tresca and R. Lefferts, *Scintillator diagnostics for the detection of laser accelerated ion beams*, *Journal of Instrumentation* **9** (2014) P09004.

[12] O. Adriani et al., *Light yield non-proportionality of inorganic crystals and its effect on cosmic-ray measurements*, *JINST* **17** (2022) P08014 [2207.06696].

[13] N.V. Mokhov and C.C. James, "The MARS code system user's guide version 15(2016)." FERMILAB-FN-1058-APC, February, 2017. 10.2172/1462233.

[14] C. Ahdida et al., *New capabilities of the FLUKA multi-purpose code*, *Front. in Phys.* **9** (2022) 788253.

[15] T. Sato et al., *Recent improvements of the particle and heavy ion transport code system – PHITS version 3.33*, *J. Nucl. Sci. Tech.* **61** (2024) 127.

[16] K. Niita, H. Takada, S. Meigo and Y. Ikeda, *High-energy particle transport code NMTC/JAM*, *Nucl. Instrum. Meth. B* **184** (2001) 406.

[17] E.D. Marquardt, J.P. Le and R. Radebaugh, *Cryogenic material properties database*, in *Cryocoolers 11*, R.G. Ross, ed., (Boston, MA), pp. 681–687, Springer US (2002), DOI.

[18] R.A. Yildiz and S. Yilmaz, *Stress-strain properties of artificially aged 6061 Al alloy: Experiments and modeling*, *J. of Materi Eng and Perform* **29** (2020) 5764.

[19] United States Office of the Federal Coordinator for Meteorological Services and Supporting Research, *Federal Meteorological Handbook No. 1 - Surface Weather Observations and Reports* (2019).

[20] P.M. Pauley, *An example of uncertainty in sea level pressure reduction*, *Weather and Forecasting* **13** (1998) 833 .

[21] C. Tegeler, R. Span and W. Wagner, *A new equation of state for argon covering the fluid region for temperatures from the melting line to 700 K at pressures up to 1000 MPa*, *Journal of Physical and Chemical Reference Data* **28** (1999) 779.

[22] J. Fernández-Varea, R. Mayol, J. Baró and F. Salvat, *On the theory and simulation of multiple elastic scattering of electrons*, *Nucl. Inst. Meth.* **B73** (1993) 447.

[23] G. Wentzel, *Zwei Bemerkungen über die Zerstreuung korpuskularer Strahlen als Beugungserscheinung*, *Z. Phys.* **40** (1926) 590.

[24] V.N. Ivanchenko, O. Kadri, M. Maire and L. Urban, *Geant4 models for simulation of multiple scattering*, *J. Phys. Conf. Ser.* **219** (2010) 032045.

[25] G. Soti, F. Wauters, M. Breitenfeldt, P. Finlay, I. Kraev, A. Knecht et al., *Performance of Geant4 in simulating semiconductor particle detector response in the energy range below 1MeV*, *Nucl. Inst. Meth.* **A728** (2013) 11.

[26] A. Makarova, B. Gottschalk and W. Sauerwein, *Comparison of Geant4 multiple Coulomb scattering models with theory for radiotherapy protons*, *Physics in Medicine and Biology* **62** (2017) 5959–5974.

[27] DUNE collaboration, *The DUNE Far Detector Vertical Drift Technology, Technical Design Report*, *JINST* **19** (2024) T08004 [2312.03130].